Study of high efficiency small diameter annular wind turbines by means of CAE techniques

Francesco Pitzalis, Nicola Corino,
Marco Ottella, *Member IEEE* and Pietro Perlo
Centro Ricerche Fiat
Orbassano, Italy
marco.ottella@crf.it

Paolo Guglielmi
Politecnico di Torino
Torino, Italy
paolo.guglielmi@polito.it

***Abstract*— The report describes the design criteria for high efficiency small-scale wind turbines. While the overall wind to electrical conversion efficiency for large diameter rotors can be set at around 50%, the design of conventional wind turbines with diameters below 0,5 m is limited by air turbulence and low electrical efficiency. Coupling a ring shaped generator with ducted blades an overall efficiency of the order of 32% for a diameter of 200 mm is feasible. This together with low friction bearings allows a starting operation at wind speeds of 1m/s.**

Keywords; Wind power generation, Permanent magnet generators, Finite element methods, Brushless machines

I. INTRODUCTION

Betz's aerodynamic theory sets to 0.59 the highest possible efficiency for an ideal propeller [1]:

$$\eta_B = \tfrac{1}{2}(1+x)(1-x^2). \tag{1}$$

with:

$$x = V_{out}/V_{in} \tag{2}$$

marking V_{out} and V_{in} the wind speed after and before propeller's plane. Indeed:

$$\frac{\partial \eta_B}{\partial x} = 0 \quad \rightarrow \quad \eta_{B-\max} \approx 0.59 \tag{3}$$

Previous studies have demonstrated critical scalability of conventional horizontal axis wind turbines particularly when the external diameter falls below 0,5m, the resulting overall efficiency being typically around 10%. The scaling down is leading to two main drawbacks:

- Aerodynamic
- Electric

From an aerodynamic point of view, the efficiency limit is set near to 59% according to Betz's studies, but for a real propeller in an ideal fluid, it is a function of the ratio between blade tip to wind speeds (Figure 1):

$$\lambda = \Omega r_e / V \tag{4}$$

with Ω propeller angular velocity, r_e external propeller radius and V wind speed.

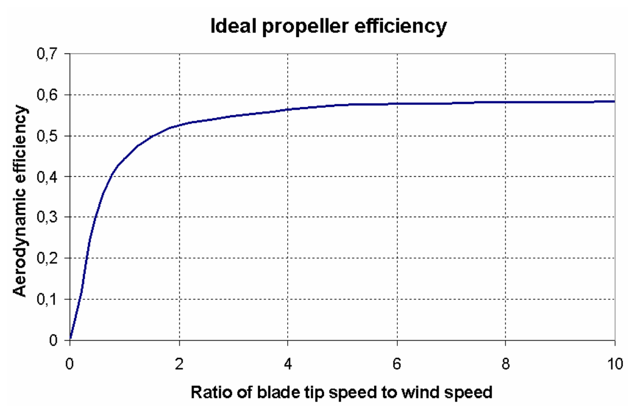

Figure 1. Graphical representation of the curve Efficiency – Ratio of blade tip speed. High values of λ are necessary to reach the efficiency limit (~59 %).

Size reduction constraints designs with low λ and therefore low efficiency, because of the difficulties to increase Ω to balance the smaller radius.

Another cause of relevant inefficiencies is Prandtl's effect (Figure 2): a single blade in a free end cannot completely guide the fluid around its shape. Vortices arises and, consequentially, blade's efficiency is reduced. The Prandtl function describes mathematically the generation of vortices decreasing the value of the angle of incidence:

$$\mathrm{FP} = \tfrac{2}{\pi} \arccos\left(\frac{1}{e^{\frac{\pi (1-r/r_e) r_e}{a}}} \right) \tag{5}$$

where FP is the value of the Prandtl's function, r_e the external radius of the blade and a the distance between the edge

This work was supported in part by the Fondazione CRT (Torino) under Grant Nanotechnology for Electromechanical Information Technology and Biomedical Industries http://www.cdcmp.it/nanotech/.

of the vortex produced by the extremity of the blades and the centre of rotation.

The effective angle of incidence can be evaluated with the following equation:

$$i_e = FP i_\infty \quad (6)$$

where i_∞ is the theoretical angle of incidence.

As result of Prandtl effect, the aerodynamic efficiency in the external portion of the blade drops to zero

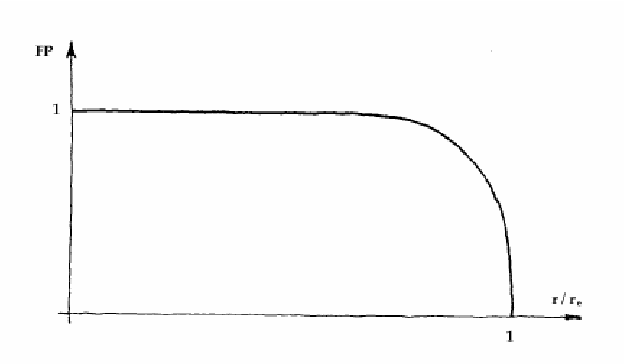

Figure 2. Value of the Prandtl function. It drops to zero near the free blade's extremity

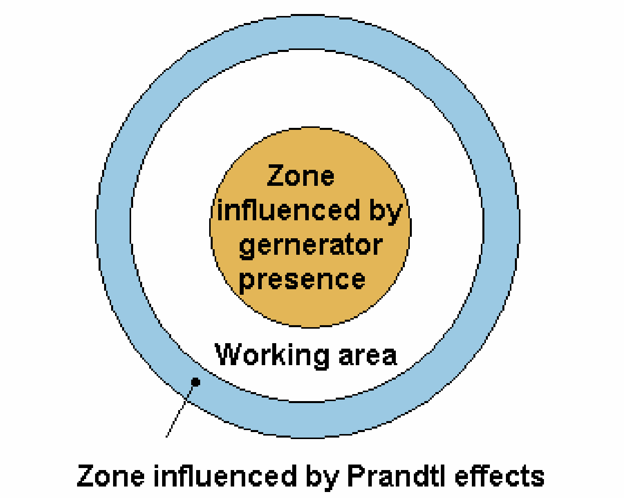

Figure 3. Zone division of propeller surface.

The presence of the generator in the centre of the turbine, is a further cause of aerodynamic inefficiencies: it occupies a volume in the axial zone of the propeller and is usually set behind the propeller itself. For a high-diameter propeller this results in a negligible effect on the overall efficiency both because the area covered by the generator is a small portion of that covered by the blades and because in the central zone the relative speed between fluid and blade is low. On the contrary, for low-diameter wind turbines, the generator hides a substantial surface of the propeller's area and the fluid flow is distorted behind the propeller.

Combining the two effects, the area of a conventional propeller can be divided in 3 zones (Figure 3):

- An external zone characterized by Prandtl's effect (low efficiency);
- a central zone where the blades are working in nominal conditions;
- an internal zone with low efficiency because of the presence of the generator.

Resizing a wind turbine to small diameters, the internal zone proportionally increases, reducing the area of high efficiency.

By this study we demonstrate that small-sized wind turbines can be designed overcoming both aerodynamic and electrical drawbacks. The proposed configuration is based on a ring shaped multipole generator and ducted blades profiled for max efficiency at 5 m/s and start-up at a wind speed of 1 m/s.

Rotor blades and the electrical generator are modeled respectively by CFD (Ansys Fluent) and FEM techniques (Cedrat Flux 2-3D).

II. Proposed Solution

Because of the described low efficiency of small-sized wind turbines, various solutions have been proposed, for example combining turbines with piezoelectric thick film stacks [4], [5], [6]. However these approaches based on the use of smart materials, because of the intrinsic limits of the materials do not allow an overall high mechanical to electrical efficiency.

In working condition (wind speed in the order of 5-7 m/s) and especially during start-up, low kinetic energy is available in the fluid (7), for example at (~5 m/s) over a circle of 0.03 m^2 the power is around 2.4 W:

$$P = \frac{1}{2} \cdot \rho \cdot A \cdot V^3 \quad (7)$$

with ρ air density, A propeller area and V wind speed.

It is then necessary to reduce all possible causes of loss in order to get a usable amount of energy.

To avoid extremity vortices the propeller can be inserted in a duct to avoid the fluid to bypass the blade. As the propeller is ducted, vortices don't arise, and losses connected with friction and laminar flows at the boundary are much smaller than Prandl's effect.

In our proposed configuration, at a rated wind speed of 5 m/s imposing an angular speed of 75 rad/s of the propeller, the Reynolds number (Re) is very low around 10'000. This is a critical condition as fluid current stays in a transition state between laminar and turbulent flow where a fully developed turbulent flow would be preferable as fluid doesn't waste energy to overcome internal frictions (viscosity). On the contrary low Reynolds numbers are typical of fluid flows where viscosity friction is much more relevant than kinetic energy of the molecules (turbulence); the efficiency of the wing profile is lower in that it can be represented as an increase of drag on the airfoil. This high viscosity of the fluid causes a dead fluid zone around the wing's surface, so that a layer of fluid is attached to the wing and in a situation of absence of relative speed fluid-blade. This causes the moving fluid stream to behave like if an alteration in the shape of the airfoil (a bigger, smoothed surface) occurs.

Due to the lack of similar examples at such low Reynolds numbers detailed CFD simulations on the wing profile have been performed by Ansys-Fluent. In accordance to [3] we selected the airfoils, GM15, E214 and WASP (designed for *Re* ~ 60'000) and the simulations demonstrated that their performance at *Re* ~ 10'000 (propeller operating condition) are quite similar.

Figure 4. Low Reynolds number airfoils [3]. From top to bottom E214, GM15 and WASP

This is because it arises a dead fluid zone around the profile thus smoothing the real airfoils shape (Figure 5); besides at the trailing edge the influence of that dead zone is relevant.

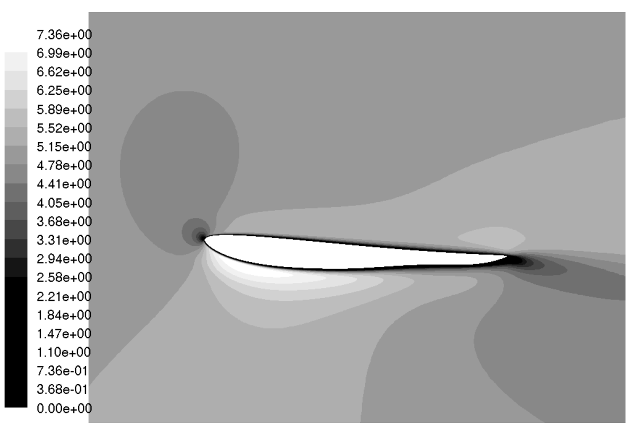

Figure 5. Fluid flow (coloured by velocity magnitude) around airfoils WASP with *Re* ~ 10'000 and wind speed 5 m/s with 9° as angle of incidence. The dark area represents the dead zone, which is particularly thick at the trailing edge.

Under such condition, the difference of the two airfoils is minimum and does not allow a discrimination between the overall efficiencies of the propellers. We can conclude that a well-designed and manufactured trailing edge is useless in that it is automatically smoothed by the dead fluid zone. Then an elliptic profile having two leading edge has been considered as this allows the propeller to be symmetric from the two axial directions of the fluid flow.

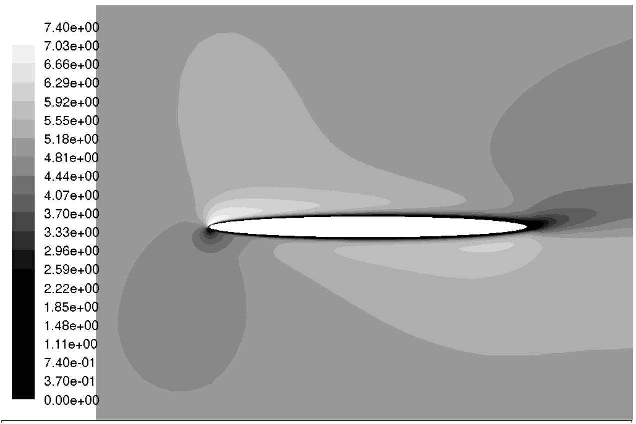

Figure 6. Fluid flow (coloured by velocity magnitude) around the elliptic airfoil with *Re* ~ 10'000 and wind speed 5 m/s with 6.5° as angle of incidence.

The studied solution is an elliptic wing profile having axes ratio set to 15: although CFD simulation shows decreasing performances, in comparison with E214, GM15 and WASP, it has been selected because it can run at both axial directions of the fluid. (Figure 6).

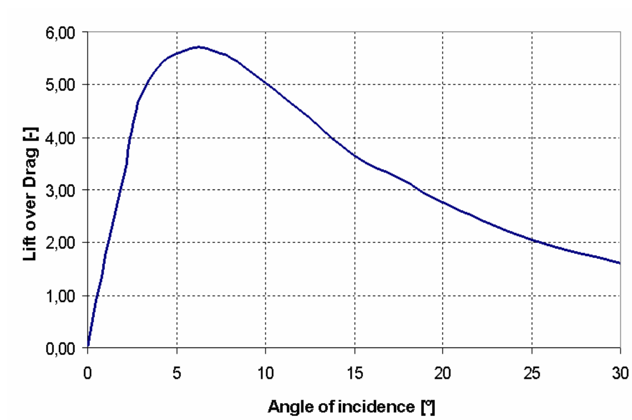

Figure 7. Wing profile Lift to Drag ratio for different angle of incidence as result of Ansys Fluent simulations for the chosen profile

The efficiency of a wing profile is given by the ratio between Lift and Drag forces for a particular angle of incidence of the fluid flow. Again for the elliptic airfoil the efficiency curve (Figure 7) has been obtained by mean of CFD simulations; the highest usable efficiency zone results at around 5°, as stall condition occurs at around 7°.

The design of the blade is performed by optimizing the blade shape for a rotating speed of 75 rad/s and wind speed 5 m/s calculating the velocity triangle in 50 blade's section for varying distance from the center of rotation (Figure 8).

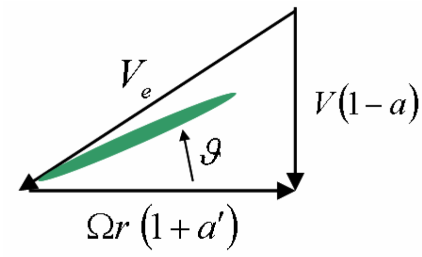

Figure 8. Triangle of velocity at a given radius (r).

The algorithm gives the values of stagger angle θ and chord (c) for each of the 50 considered radius in order to make the profile working with the highest Lift over Drag ratio in the optimum conditions. In Figure 8 the parameters *a* and *a'* represent the axial flow slowdown at the blade plane, and the vortex ration of the flow after the interaction with the blades. These values are mathematically defined for the optimum working point. Further improvements of the model has required Bezier interpolation of the continuous functions

$$\begin{cases} \vartheta = f(r) \\ c = f(r) \end{cases} \tag{8}$$

In this assembly, a ring shaped electrical machine allows a high efficiency multipole configuration (Figure 5). This also permits a direct-drive concept [7] even at low rotational speed (typically 75-100 rad/s) and consequently high efficiency at small diameters. The direct drive concept has also been proven in previous studies to show good efficiency figures [8].

Figure 9. Example of a wind turbine assembly (no similitude with studied model)

To find an optimal solution four options have been compared in terms of performance and cost:

- Conventional brushless SPM architecture: a simple low-cost solution suffering the drawback of a high rotor inertia (due to the presence of an iron ring in the rotor), high cogging torque and higher losses (mainly iron core);
- Slotless stator: reduces cogging and iron core losses, but still suffering of high rotor inertia;
- Halbach array rotor: known [9] to associate low weight/inertia and low cogging, also presenting good losses figures.
- Ironless hallbach rotor (best in class in terms of efficiency)

Machine characteristics are summarized in Table I, each having 12 poles, 3 phases and each being designed as a starting point at 12V, 700mW output at a rated speed of the propeller of 75 rad/s. A fill factor in the order of 0.3-0.4 have been considered both in the slotted and in the slotless structure, although manufacturing processes allow much higher fillings in slotless structures.

In addition the three-phase rectifier circuit have been simulated by Flux2D, considering Schottky diodes having 13 mΩ on-resistance.

On the rotor, plastic bonded permanent magnets, viz. Saimag GPM12L, have been considered in the iron core structure and Sintered NdFeB, viz. Saimag N-45 in the ironless one.

TABLE I. ELECTRICAL MACHINES SUMMARY

Machine characteristics	**Machine type**			
	Slotted	***Slotless***	***Hallbach***	***Ironless***
Per phase turn number	180	480	480	504
Stator external radius (mm)	135	135	135	131
Rotor internal radius (mm)	117	119	120	121
Airgap radius (mm)	125	125	125	125
Airgap thickness (mm)	0.5	1	1	1
Iron core	Silicon Steel	Silicon Steel	Silicon Steel	
Magnets	Bonded NdFeB	Bonded NdFeB	Bonded NdFeB	Sintered NdFeB

III. ANALYSIS METHOD

The wind turbine has been modelled with Matlab/Simulink considering the second-order system:

$$J\dot{\omega} + T_R + T_E = T_B \tag{9}$$

being J the inertia of the rotor, ω the angular acceleration and T_B the torque generated by the blades, T_R the friction torque ant T_E the electrical load (electrical machine, rectifier, load).

The blade motion torque is calculated in a separate block that performs an internal iteration to define the characteristics of the triangle of velocity at a given radius; at each iteration the triangle of velocity is solved and values of *a* and *a'* (Figure 8) are calculated. As the triangle of velocity defines the angle of incidence at which the relative wind encounters the airfoil, Lift and Drag forces become known. These, integrated, give the torque generated by the turbine (T_B).

Finally the electrical torque (T_E) is calculated my means of coupled field calculation, using Maxwell Stress Tensor.

A first simulation run has been performed in order to compare startup speeds of different embodiments. As the generator is designed to startup at 1m/s wind speed and for maximum efficiency at 5m/s, the time needed to reach the rated speed of propeller at 75 rad/s for the 5m/s of wind speed has been calculated, taking into account the overall rotor inertia, the dynamic turbine behaviour and friction.

As a second stage, detailed analyses to determine maximum efficiency have been performed at a rated wind speed of 5 m/s by means of strongly coupled mechanical-field-circuit simulations [13] using Matlab/Simulink and Cedrat-Flux 2D/3D. Specifically electrical efficiency has been evaluated calculating the mechanical power flowing into the generator and the electrical power on the resistive load (10)

$$P_{el} = \frac{1}{T}\int_0^T i(t)v(t)dt \qquad (10)$$

Winding Joule losses have been modelled as series resistances into the winding circuit and rectifiers losses have been modelled as resistances with a threshold voltage.

In addition, at the end of simulation, iron core losses have been estimated using a simplified Bertotti's formulation and magnetic field calculated by Flux2D/3D

$$P_{core} = \iiint_{volume} dP_{moy}\, dV \qquad (12)$$

$$dP_{moy} = \frac{1}{T}\int_0^T dP(t)dt\,. \qquad (13)$$

$$dP(t) = \left[k_h B_m^2 f + \frac{\sigma d^2}{12}\left(\frac{dB}{dt}(t)\right)^2 + k_e\left(\frac{dB}{dt}(t)\right)^{3/2}\right]k_f \qquad (14)$$

where

- k_h is the coefficient of hysteresis losses
- k_e is the coefficient of excess losses
- σ is the conductivity of the material
- δ is the lamination thickness
- f is the frequency
- B_m is the peak value of the magnetic flux
- k_f is the coefficient of filling of the magnetic core.

IV. Results and Discussion

Preliminary FEM calculation, performed at no load, showed that a slotted architecture is not suitable as its cogging torque overrides blade torque, braking the turbine at start-up. Besides the small axial length does not allow skewing.

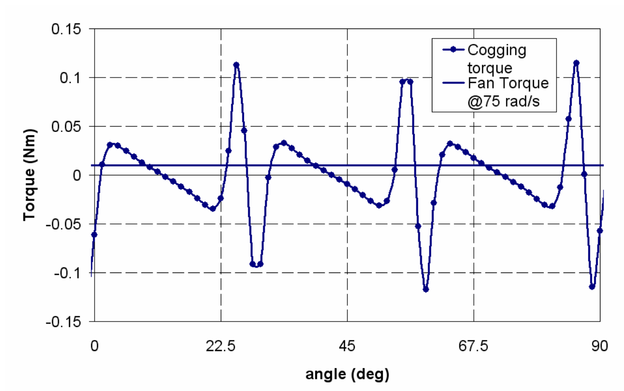

Figure 10. Cogging torque of slotted electrical machine

Neglecting iron losses, all generators considered would have very good efficiency, as summarized in Table II

TABLE II. Simulation Results

Simulation results	Machine type		
	Slotless	***Hallbach***	***Ironless***
Wind Power (mW)	2400	2400	2400
Rotor Inertia (kg·m^2)	12.1x10^{-3}	11.3x10^{-3}	10.5x10e^{-3}
Startup time (s)	51	49	46
Output Power (mW)	296	321	720
Joule Losses (mW)	51	51	53
Iron core losses (mW)	428	403	0
Total Losses (mW)	479	454	53
Electrical Efficiency	38%	41%	93%
Overall Efficiency	12.3%	13.4%	30.0%

As it can be noticed looking at Figure 11 and Figure 12, both machines match good design criteria; induction in stator and rotor iron remains at reasonable levels. However these two solutions, both comprising a ferromagnetic stator, show low efficiency values (in the order of 40%), in that iron losses (mostly hysteresis) arise in the stator as soon as the machine starts rotating. In addition this effect would brake the turbine thus prolonging start-up time much more than predicted by simulation.

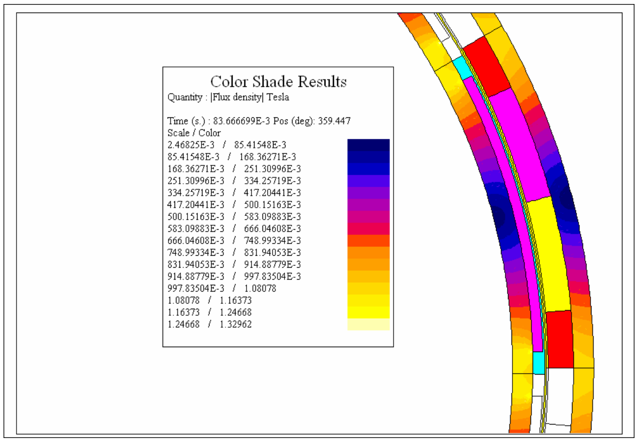

Figure 11. Slotless machine induction map (one pole)

A solution with an Hallbach array rotor and ironless stator, completely cancelling iron core losses, leads to an overall efficiency of 30%. As this would be an expensive solution efforts could be made in the direction of cost reduction by adopting conventionally magnetized rotor, plastic bonded NdFeB magnets and ironless stator.

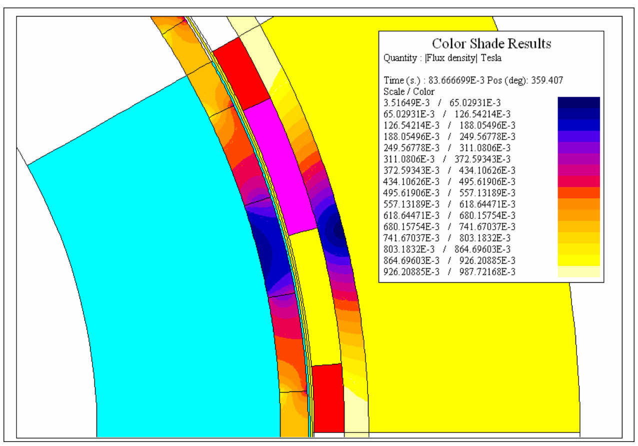

Figure 12. Hallbach array machine induction map (one pole)

Simulations have also been made on the use of soft magnetic composites, viz. Höganäs Somaloy™500, + 0.5% Kenolube, compressed at 800MPa and cured at 500 °C [14], allowing light weight, and showing the highest potential in terms of cost reduction, making stator assembly easier and thus low cost. Magnetization characteristics of Somaloy™ in comparison with laminated silicon steel is shown in Figure 13.

Although SMC has a much lower permeability than silicon steel, it does not reduce flux linkage significantly in that slotless structures and permanent magnets behave like air under magnetic flux. Furthermore SMC shows the drawback of hysteresis losses (see Table III) much higher than those of silicon steel..This makes SMCs unsuitable for a small low power high efficiency electrical machine like the one here proposed.

TABLE III. IRON LOSSES COEFFICIENTS USED IN THE SIMULATIONS

Iron losses coefficients	**Iron core**	
	Silicon Iron	***Somaloy™ 500***
k_h (Ws/Tm^3)	120.9	964
σ (S/m)	1.33x10^6	9803
k_e (W[Ts^{-1}]$^{-3/2}$m^{-3})	0.78	1.466
δ(mm)	0.35	10

However a good compromise between cost and efficiency that considers a rotor comprising an iron core made by SMC together with convetional magnets is technically feasible; allowing a one step manufacturing by bonding magnets and iron core together followed by a magnetisation process.

Finally to allow a quasi-zero friction, a combination of passive conic shaped magnetic bearings [11], air foil bearings [12] and plastic bearings can be considered. This solution can overcome known stability problems of passive magnetic bearings when used alone, thus maintaining low friction. Infact air-foil bearings are designed to be active only at startup, thus leaving magnetic bearings (stabilized by gyroscopic effects) centered at rated speeds.

However, as a matter of completeness, dynamic simulation considered a small friction of some hundreds of micro Newton

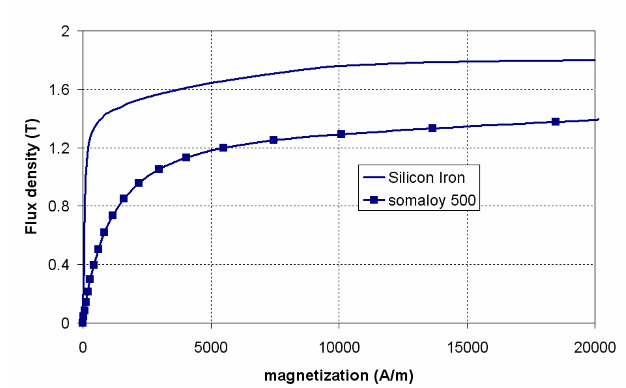

Figure 13. Magnetization characteristics of Somaloy™ in comparison with the silicon steel

V. ARRAY CONNECTION

The device itself is capable of supplying small electrical loads, for instance to a network of autarkic wireless sensors or to charge a variety of personal devices.

The advantage of this solution is its low cost fabrication. Problems arises for electrical connection of a multitude of generators in an array; for example each bridge rectifier in a series connection have to support the overall load current (Figure 14). On the other hand, in a parallel array connection (Figure 15) each generator must supply the same voltage, otherwise only the generator with the highest voltage would give power while other generators would remain in idle state.

This has to be taken into great concern because the generators are exposed to different wind flows.

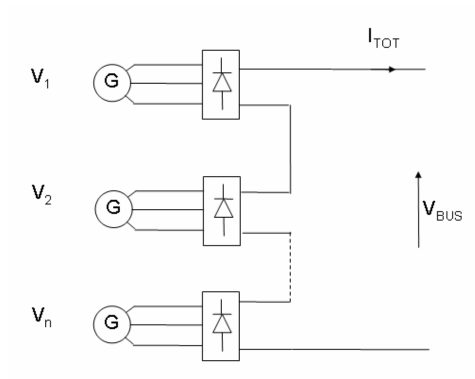

Figure 14. Series connection of multiple wind turbines

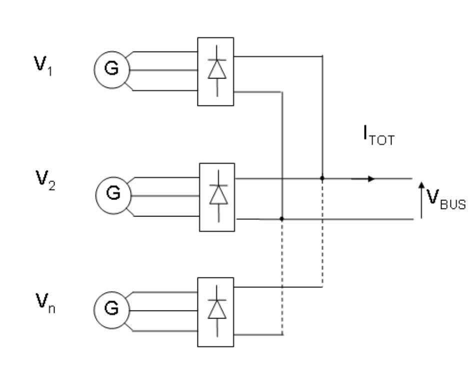

Figure 15. Parallel connection

To overcome this problem a DC/DC converter at each generator could be used even if it would lead to increased complexity and cost. The proposed configuration allows a very small increase in power electronics complexity and consists in a series connection of N generators, each designed for low current and high voltage, with a single DC/DC converter (Figure 16).

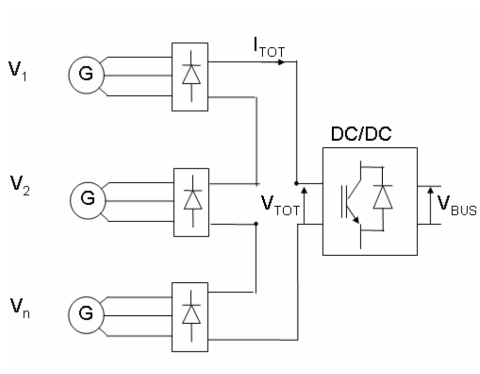

Figure 16. Series connection of wind turbine array + DC/DC converter

Dynamic behaviour of in series array connection of wind generators (four turbines) have been performed by means of a weakly coupled FEM-simulink simulation: the characteristic parameters of the electrical machine have been calculated by FEM, and simulations have been performed off-line by Simulink.

As predicted series connection guarantees optimal connection for all four generators exposed to varying and different wind conditions such as shown in fig 17.

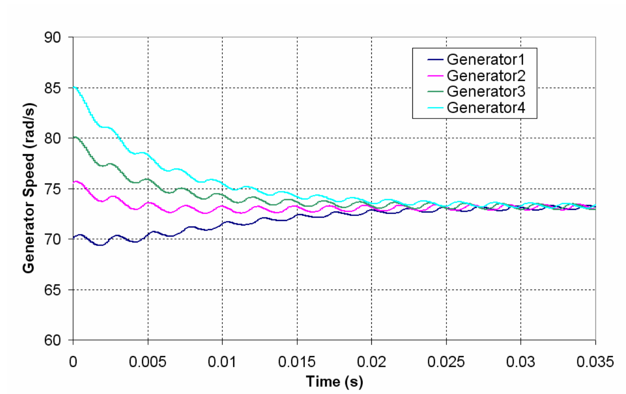

Figure 17. Array connection of four generators

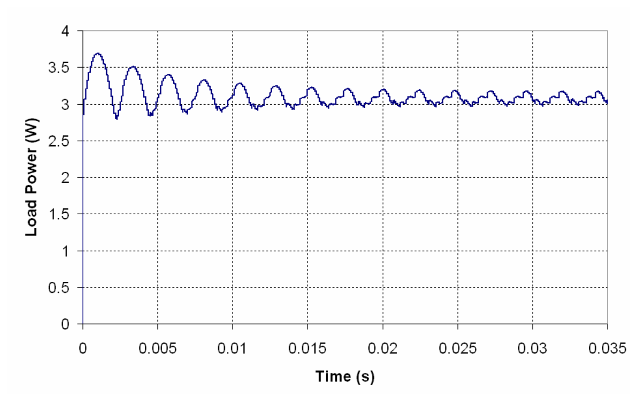

Figure 18. Array connection of four generators: overall output power

ACKNOWLEDGMENT

The Authors want to acknowledge Daniele Zanello for his precious help in simulations. They especially want to mention Fondazione CRT in the person of Mr. Lorenzo Gianotti for continuous support of the project.

REFERENCES

[1] G. A. Pignone and U. R. Vercelli, Turbomacchine, Milano: Editore Ulrico Hoepli, 1991.

[2] “Wind turbine – Part 12: Power performances measurements of electricity producing wind turbines”, IEC, IEC 61400-12-1, 2005

[3] M. S. Selig, J. J. Guglielmo, A. P. Broeren and P. Giguère, Summary of Low-Speed Airfoil Data, Vol. 1, SoarTech Publications, 1995

[4] S. Priya, C. T. Chen, D. Fye and J. Zahnd, “Piezoelectric Windmill: A Novel Solution to Remote Sensing”, Japanese Journal of Applied Physics, Vol. 44 - No. 3 2005, pp. L 104–L 107, 2005

[5] Perlo P., Butera F., Alacqua S., Zanella A. and Carvignese C., “Dispositivo generatore elettrico con pannello recante una distribuzione di mini-generatori eolici”, IT Patent TO2001A000386, Apr. 24, 2001

[6] Zanella A, Butera F., Perlo P., Alacqua S., Biasiotto and M., Perosino A., “Electrical Energy Generator Device With Micro-Fan Array”, U.S. Patent 2006/0012264, Dec. 23, 2003

[7] Chen J., Nayar C.V., Xu L., “Design and Finite-Element Analysis of an outer-rotor permanent-magnet generator for directly coupled wind turbines”, IEEE Transaction on Magnetics, Vol 36, No. 5, pp. 3802-3809, 2000

[8] H. Polinder, F.F.A. van der Pijl, G.J. de Vilder, and P. Tavner, “Comparison of direct-drive and geared generator concepts for wind turbines”, in Proc IEEE Int. Conf. Electric Machines and Drives, San Antonio, USA, 2005, pp. 543-550.

[9] Jang S., Jeong S., Ryu D., Choi S., “Design and analysis of high speed slotless PM machine with Halbach array”, IEEE Transaction on Magnetics, Vol 37, No. 4, pp. 2827-2830, 2001

[10] Canova A., Gruosso G., Ottella M, Repetto M. and Schofield N., “Soft Magnetic Composites for tubular linear actuators”, in Proc. Internationa Conference on Electrical Machines, Brugge, 2002, Vol. CD-Rom, 2002

[11] Bassani R., Ciulli E., Di Puccio F., Musolino A., “Study of conic permanent magnet bearings”, Meccanica, No. 36, pp. 745-754, 2002

[12] Agrawal G.L., “Foil Air/Gas Bearing Technology – An Overview”, ASME Publication, 97-GT-347 pp. 1-11, 1997

[13] Canova, A., Ottella M. and Rodger, D., “A coupled field-circuit approach to 3D FEM analysis of electromechanical devices”, in Proc 9th International Conference on Electrical Machines and Drives, 1999, pp. 71 – 75

[14] Wang, J., Howe, D., “Influence of soft magnetic material on the design and performance of tubular permanent magnet machines”, IEEE Transactions on Magnetics, Vol. 41, No. 10, pp. 4057-405